Title
Considerations for Variable Timestep Integration in Hamiltonian Dynamics

Author
Pereyra, Carlos

Publication Date
2023

Peer reviewed|Thesis/dissertation

Considerations for Variable Timestep Integration in Hamiltonian Dynamics

By

CARLOS Z. PEREYRA

THESIS

Submitted in partial satisfaction of the requirements for the degree of

MASTER OF SCIENCE

in

Mechanical and Aerospace Engineering

in the

OFFICE OF GRADUATE STUDIES

of the

UNIVERSITY OF CALIFORNIA

DAVIS

Approved:

Niels Grønbech-Jensen, Chair

Jean-Jacques Chattot

Davide Donadio

Committee in Charge

2023

Contents

Considerations for Variable Timestep Integration in Hamiltonian Dynamics

Abstract

While great advances have been made in the field of intermolecular potentials for molecular modeling and material science, the choice in constant energy integration dynamics have been often relegated to the Størmer-Verlet. In the past 30 years the symplecticity of this method and relatively low local error in initial conditions have made this integrator a hallmark of stability. However, the need to perform N-body particle simulations to reach greater time domains has encouraged practitioners to approach higher timesteps and the stability limit.

This article explores implicit classes of adaptive Verlet algorithms for potential use in the two-stage coupled equations of motion. At the heart of these methods are state dependant, time re-scaling functions that offer bounded variable timesteps. There is not many demonstrations of their overall energy conservation for a choice in timestep value, beyond global error demonstrations in discrete time. Presented here is the derived linear stability for arbitrary time transformation functions with the implicit Adaptive Verlet scheme. Considerations for selecting a stable range of timesteps in fulfilling stable harmonic trajectory are also outlined.

Lastly we observe evidence that the implicit Adaptive scheme paired with a bounded timestep model may contain a family of solutions that contribute additional spectral elements. Regular modes of spectral peaks shown in our monochromatic system point towards additional solutions in the Hamiltonian system. Before moving towards variable timestep methods we demonstrate the need to develop a transformation functional that meets symmetric criteria outlined by previous authors.

Acknowledgments

I give thanks to my major advisor Dr. Niels Grønbech-Jensen, whom I have enjoyed learning from and sharing new ideas with. I am grateful to have met my committee members and to have their guidance. The experiences here at UC Davis have built up my curiosity for numerical techniques and exploring new methods.

In my personal life I am infinitely grateful to my parents for instilling me with a sense of joy for mathematics and computer programming. To those who have helped me move several times while I was working on this, I give immense thanks. Lastly, I give thanks to everyone whom I've had conversations with during the pandemic years of my graduate experience.

Nomenclature

$\mathcal{M}$	Diagonal mass matrix
k	Pendulum spring constant
m	Mass
s	Time transformation functional
W	Maximum timestep ratio
w	Minimum timestep ratio

CHAPTER 1

Introduction

In this document we consider the application of symplectic and time reversible variable timestep integrators of the Verlet type. The work performed here intends to demonstrate the limitations of variable timestep methods in transient stability and frequency response. It is the hope that with these methods, progress towards reaching greater time domains and higher stability can be achieved with optimal timestep scaling, that can potentially outperform current practices deployed in models that require timestep adjustments.

Such cases that may require adaptive variable integration timesteps include the field of advanced intermolecular potential development. More recent advances towards deep learning potentials that are reliant on ab-initio calculations called density functional theory have expanded models beyond pairwise differences and have offered greater insights into invariant atom representations [**5**] [**3**]. This work has pioneered predictive accuracy in fusion containment materials for the ITER experiment and intermetallic materials [**30**] [**32**] [**10**]. With these increases in model complexity, arises greater computational expense in calculating atomistic forces [**34**] [**25**]. As potentials become more complex, the need to develop integrators for nominally higher integration steps can help us avoid the number of calculations required to reach greater time domains. Presented here are algorithms used to systemically alter the timestep through use of a modified constant energy Hamiltonian.

The usual description of N body dynamics through the Hamiltonian dictates that the total energy $H = T + V$ is a constant for d dimensional position $\boldsymbol{q} \in \mathbb{R}^{d \times N}$ and momenta $\boldsymbol{p} \in \mathbb{R}^{d \times N}$ vectors. The kinetic energy T and general state dependent potential $V(\boldsymbol{q})$ define the coupled set of linear differential equations in (1.1).

$$\begin{aligned} \frac{d\boldsymbol{q}}{dt} &= H_{\boldsymbol{p}} \\ \frac{d\boldsymbol{p}}{dt} &= -H_{\boldsymbol{q}} \end{aligned} \tag{1.1}$$

This relation can be seen defined more explicitly in equation (1.2).

$$
\begin{aligned}
H_{\boldsymbol{p}} &= \frac{\partial T}{\partial \boldsymbol{p}} = \mathcal{M}^{-1}\boldsymbol{p} \\
-H_{\boldsymbol{q}} &= -\frac{\partial V}{\partial \boldsymbol{q}} = -\nabla V(\boldsymbol{q})
\end{aligned}
\tag{1.2}
$$

A great deal of effort goes into determining the model potential V that drives the forces $f = -\nabla V(\boldsymbol{q})$. Traditionally models have been empirically derived and relate closely to quantum mechanical perturbation theory. The Lennard Jones family accurately describes equilibrium properties in liquids for noble elements by determining second order virial coefficients [**24**] [**31**]. Another example is the Ziegler Biersack Littmark (ZBL) potential which accounts for electronic screening and gets repulsion very well for metals [**33**].

In many cases Molecular Dynamic (MD) simulations employ linearly discrete time integrators to solve (1.2) and to predict the evolution of position and velocity for a system of many particles. The time evolution can reveal valuable insight into not only ergodic ensemble properties, but also periodic dynamical behavior. Ab-initio based MD simulation have proved to be invaluable in observing vibrational phenomena seen at long time scales on the order of sub-nanosecond. Such an example is seen in long-time dynamical simulations of 1,3,5-trinitroperhydro-1,3,5-triazine where low frequency modes that were not observable at the picosecond scale were resolved at higher time scales [**9**]. Thus it is the goal here to explore adaptive integrators as a more efficient method of achieving long time integration in the microcanonical ensemble.

The adaptive methods presented herein are of the Verlet type and descend from the second order Størmer-Verlet (SV). The Verlet method often serves as a basis for many types of integrators intending to find position q and momentum p, since the phase space area is preserved in time and obeys time-reversibility for fixed timestep h [**16**]. It can also be shown that the SV method is a special case of the 2-stage Runge-Kutta or Lobatto IIIA-IIIB formulation [**27**] [**6**] that uses terms from essential tableau's satisfying the symplectic characterization of discrete integrators [**13**].

The SV method is an excellent choice for any fixed timestep MD simulation. Though in some cases when it becomes necessary to vary the timestep based on the potential energy, all symplectic properties are lost due to violations in the geometric construction. Calvo et. al computationally

demonstrates that changes to the timestep during Verlet integration voids symmetry and symplecticity [**8**] [**16**]. Although it is desirable to shift the timestep as a function of the potential's curvature for optimal stability, the consequences in fixed timestep methods are given by an exponential growth in error [**14**]. Despite this issue, the practice of variably shifting the timestep to accommodate high energy situations is often employed for ion implantation studies [**4**] [**17**] [**10**]. This is where the adaptive methods show here may address the needs of the material science community.

1.1. Time Transformations

Let us begin by examining how dynamical systems change with a time transformation. We first consider here a time-transformation that takes the ordinary differential equation of f

$$\begin{aligned} \frac{dt}{dt} &= 1 \\ \frac{dx}{dt} &= f(x) \end{aligned} \tag{1.3}$$

into an artificial time frame, where now s describes the time scaling relation.

$$\begin{aligned} \frac{dt}{d\tau} &= s(x) \\ \frac{dx}{d\tau} &= s(x)f(x) \end{aligned} \tag{1.4}$$

E. Hairer shows the relation $s(x)$ was used extensively in the search for an analytical solution to the Kepler three body dynamics problem [**29**, p. 127] [**23**, p. 313] [**15**]. Stoffer shows that it is possible to choose a scalar function $s > 0$ such that integration of (1.4) from 0 to a small timestep ε maps one to one with the integration of (1.3) with a variable step $[0, \varepsilon s(x)]$. Essentially a discrete integration method Φ with variable timesteps applied to (1.3) maps to a variable flow method $\tilde{\Phi}$ with fixed discrete width ε. More details on Stoffer's work on time invariance between the ordinary differential equation in (1.3) and the system in (1.4) may be referred to here [**28**].

Admittedly the adaptive Verlet techniques that vary the timestep here are not integrating the usual Hamiltonian instead we make use of another timeframe τ and thus another Hamiltonian $\tilde{H}$ [**15**].

$$\tilde{H} = s(q,p)\,(H - \gamma) \quad \text{and} \quad H = 1/2p^T M^{-1} p + V(q). \tag{1.5}$$

As a consequence of this transition, a new set of differential equations are formulated. These modified equations of motion are referred to as *Sundman* time transformations and shown below.

$$\begin{aligned} \frac{dq}{d\tau} &= s(p,q)H_p \\ \frac{dp}{d\tau} &= -s(p,q)H_q \end{aligned} \tag{1.6}$$

Formulating an integrator of the symplectic kind for *Sundman* transformations is a difficult task due to non-linear terms introduced by s. However, the functional s may be leveraged to vary the timestep such that it is sensitive to the model curvature. Ensuring that this variation is time reversible is the topic for the next section.

1.2. Time Reversibility Criteria

In order to use variable timesteps without breaking time symmetry, we introduce the criteria for maintaining time invariance and flow symmetry. Regardless of the treatment of the Hamiltonian, there are constraints on choosing the particular time transformation function.

The notions of satisfying symmetry or time-reversibility within a variable timestep method are subtle and are not necessarily the same as demonstrating symplecticity. For instance showing general time-reversibility in a one-step flow method $q_{n+1} = \Phi_h(q_n)$ does not guarantee area preservation of phase space. Going into further detail on the topic of symplecticity is outside the scope of this document and can be found in E. Hairer's textbook [**16**]. Focused here in this section are the qualities that the methods shown in Chapter 2 must meet in order to satisfy time reversibility.

The criteria for one-step flow symmetry begins with the concatenation of flows in equation (1.7) for some integration timestep h.

$$\Phi_h \circ \Phi_{-h} = I \tag{1.7}$$

Taking the above relation one step further, it is useful to show time symmetry through the equivalence of the original flow method and its adjoint $\Phi_h^* = \Phi_{-h}^{-1}$ [**16**]. This can be seen by the relation (1.8) which demonstrates that a reversal of timestep h signage and a swap of $q_{n+1} \leftrightarrow q_n$ arrives at

the original flow expression for symmetric methods.

$$\Phi_h = \Phi_{-h}^{-1} \tag{1.8}$$

Let it be known that the superscript suggests time and thus the -1 suggests the previous timestep. The subscript h defines the timestep, where the minus sign literally changes the sign in front of h within the integration method Φ. It is an interesting exercise to show the *implicit mid-point method* satisfies the criteria $q_1 = \Phi(q_0) \longleftrightarrow \Phi(q_1) = q_0$ and thus meets time symmetry despite not being a symplectic method.

In all of these steps the time scaling function is not mentioned, however to maintain time symmetry we note that s must be symmetric. The requirement in $s(\boldsymbol{q}, \boldsymbol{p}) \rightarrow s(\boldsymbol{q}, -\boldsymbol{p})$ is shown by Leimkuhler [**20**] [**19**]. A solely $\boldsymbol{q}$ dependent function clearly satisfies this invariance. A notable example is provided by Levi-Cevita who uses the inverse of position $s(\boldsymbol{q}) = \|\boldsymbol{q}\|^{-1}$ as time transformation function [**23**].

Note that at this point we've shown requirements for symmetry, but not necessarily time-reversibility. The method Φ is considered time-reversible if the relation (1.9) is true, where ρ is a general operator. This relation holds if and only if Φ_h is symmetric.

$$\rho\Phi_h(q) = \Phi_{-h}\left(\rho q\right) \tag{1.9}$$

Since s is now incorporated into Φ the condition $s(\rho\boldsymbol{q}) = s(\boldsymbol{q})$ now becomes a prerequisite for time reversibility. This can also be applied to a coupled set of differential equations as shown below.

$$s(\rho\boldsymbol{q}, \rho\boldsymbol{p}) = s(\boldsymbol{q}, \boldsymbol{p}) \tag{1.10}$$

In general it is difficult for s to satisfy time-reversibility, except in cases wherein ρ is an orthogonal transformation ($\rho\rho^{-1} = I$) [**22**]. Throughout this study s is chosen such that factors of q are quadratic and thus symmetric, though awareness is given to the fact that integration may not be time-reversible despite long time integration stability shown later.

1.3. A Bounded Scaling Function for Oscillatory Motion

So how do we select a time scaling functional that abides by time symmetry and stays within given timestep limits? One such example, that is symmetric but not bounded is a coordinate invariant functional referenced by Hairer [**15**] shown below.

$$s(\boldsymbol{q},\boldsymbol{p}) = (\boldsymbol{p}\cdot\boldsymbol{p}/m + \boldsymbol{\nabla}V(\boldsymbol{q})\cdot\boldsymbol{\nabla}V(\boldsymbol{q})/m)^{-1/2} \tag{1.11}$$

The example here leverages the Hamiltonian thus the integration procedure may re-scale for both high momenta and close packed collision type situations. Note that the nominal value of s scales non-linearly as a function of q and p and may yield exceptionally large values in s. Keep in mind variable timestep methods define an effective timestep that is the product of h and $s(q)$, so an unnecessarily large s may increase the integration step beyond the stable limit. Thus to avoid this issue a new functional s_ζ was devised to provide limits on the effective timestep.

The following sections present an alternative scaling parameter that is capable of automatically yielding the minimum desired timestep in regions of extreme potential energy curvature ($\nabla V \to \infty$). A function that fits this asymptotic behavior is defined below,

$$s_\zeta(\boldsymbol{q}) = \left(\frac{\left(\|\nabla V(\boldsymbol{q})\|^2 + w^\zeta\right)^{1/\zeta}}{1/W\left(\|\nabla V(\boldsymbol{q})\|^2 + w^\zeta\right)^{1/\zeta} + 1}\right)^{-1} \tag{1.12}$$

where the timestep boundary parameters $W = h/h_{\min}$ and $w = h/h_{\max}$ were chosen so that the product with the 'fictitious' timestep h gives a value between the maximum and minimum discrete timestep.

$$h_{min} < h \circ s_\beta < h_{max} \tag{1.13}$$

This functional represents a generalized form of Leimkuhler's bounded scaling function for $\zeta = 2$, where $s_{\zeta=2}$ approaches a plateau when forces approach infinity and relaxes in regions of zero gradients. This behavior is represented in equation (1.14). Originally $s_{\zeta=2}$ was applied in Kepler

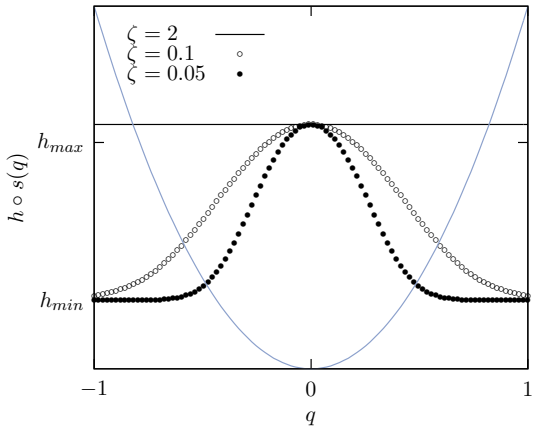

FIGURE 1.1. A representation of s_ζ for an array of ζ values. Each variation of s_ζ is plotted for the unit hooke's potential (spring constant $k = 1$) with $h_{\min} = 0.001$, $h_{\max} = 0.005$, and $h = 1$. The black curve represents the initial form of s_ζ which corresponds to $s_{\zeta=2}$. Clearly decreasing ζ allows s_ζ to vary between nominal $h_{\min}$ and $h_{\max}$ values. Note extreme values of ζ can lead to cusps.

gravitational models for time-reversible variable timestep integration [**20**].

$$\begin{aligned} \lim_{\nabla V \to \infty} s &= 1/W \\ \lim_{\nabla V \to 0} s &= 1/W + 1/w \end{aligned} \tag{1.14}$$

The functional s_ζ provides adjustable roots ζ that serve in constraining the bounds within desired limits. In total there are effectively three hyperparameters $h_{\min}$, $h_{\max}$, and ζ that provide user control in timestep range as shown in the vertical axis, while domain responsiveness is shown on the horizontal axis of Figure 1.1.

To characterize the methods in Chapter 2 the functional s_ζ must be tuned to fit within the harmonic oscillator's domain boundaries $q \in [-1, 1]$. The initial behavior of $s_{\zeta=2}$ is shown as the solid black line plotted in Figure 1.1 as a function of the quadratic potential. We initially expected this function to vary between $h_{\min}$ and $h_{\max}$ within the domain but noticed that it appears unresponsive and essentially constant. At large potential gradients (off the chart) $s_{\zeta=2}$ does smoothly vary the timesteps, meaning this configuration is be better suited for potentials with extreme gradients in curvature such as q^{-1}. Essentially to modify s_ζ for the harmonic oscillator

the first limit in (1.14) must now be tuned to,

$$\lim_{\nabla V \to k q_{max}} s = 1/W \tag{1.15}$$

where the behavior at zero gradient is automatically fulfilled.

Manually the exponent parameter ζ was tuned to approach the appropriate limit for variation, so s_ζ responds within regions of interest. Reasonable variation in s was found with $\zeta = 0.05$ and $\zeta = 0.1$ for suitable values of W and w defined in the caption of Figure 1.1. A more general approach to finding the optimal ζ value can be taken with data science techniques, but is not necessarily for the harmonic oscillator.

In general building a symmetric functional that is sensitive to arbitrary potential energy surfaces, may be determined using s_ζ. In fact many different functional forms may be used, but s_ζ serves as a symmetric and simple adjustable form that can provide boundary control over the timestep range $h_{\min}$ and $h_{\max}$. Additionally, optimization of ζ can be performed for any intermolecular potential of interest, thus providing a flexible framework for physical modelling practitioners. Finding the optimal scaling hyperparameters $h_{\min}$, $h_{\max}$, and ζ may increase the length of time per time step iteration and thus may help in potentially reaching greater time domains. Although variable timestep schemes are typically implicit there is room for high performance computing to reduce the number of additional implicit iterations but is again outside of the scope here.

CHAPTER 2

Adaptive Time Integration

We begin looking at variable timestep methods by first visiting the well known Størmer-Verlet algorithm. It has been widely used across dynamical systems for its second order accuracy in position and its computationally efficient explicit one-step methodology. When applied to the Hamiltonian equations of motion, only one force calculation per step is required in $\boldsymbol{p}_{n+1}$. It is also easy to see in (2.1)-(2.3) that the implementation of this method requires minimal memory to override and save the vector quantities $\boldsymbol{q}_n \to \boldsymbol{q}_{n+1}$, $\boldsymbol{p}_n \to \boldsymbol{p}_{n+1}$ and $\boldsymbol{f}_n \to \boldsymbol{f}_{n+1}$ at every updated timestep $n+1$.

$$\boldsymbol{p}_{n+1/2} = \boldsymbol{p}_n + \frac{h}{2m}\boldsymbol{f}_n \tag{2.1}$$

$$\boldsymbol{q}_{n+1} = \boldsymbol{q}_n + h\boldsymbol{p}_{n+1/2} \tag{2.2}$$

$$\boldsymbol{p}_{n+1} = \boldsymbol{p}_{n+1/2} + \frac{h}{2m}\boldsymbol{f}_{n+1} \tag{2.3}$$

$$t_{n+1} = t_n + h \tag{2.4}$$

More importantly the flow functions satisfy time symmetric and symplectic area preserving properties. Many authors have shown it is a special case of the Partitioned Runge-Kutta (PRK) and Lobatto IIIa-b methods [**13**]. Though this method provides long time integration stability, it is still susceptible to discrete errors in velocity depending on the given set of initial conditions [**21**]. This method is also limited to a single timestep setting in h, but may be varied at the cost of sacrificing structural symmetry properties. We consider in the next section an integrator that is structurally designed for varied timestep while maintaining time symmetry.

2.1. Implicit Adaptive Verlet

The Implicit Adaptive Verlet method (IAV) also known as the semi explicit Verlet method is derived from the fundamental PRK formulation in the same manner that is used to construct the Størmer-Verlet.

$$\varrho = \frac{s(\boldsymbol{p}_{n+1/2}, \boldsymbol{q}_n) + s(\boldsymbol{p}_{n+1/2}, \boldsymbol{q}_{n+1})}{2}$$

$$\boldsymbol{p}_{n+1/2} = \boldsymbol{p}_n + \frac{h}{2m} s(\boldsymbol{p}_{n+1/2}, \boldsymbol{q}_n) \boldsymbol{f}_n \tag{2.5}$$

$$\boldsymbol{q}_{n+1} = \boldsymbol{q}_n + h\varrho \boldsymbol{p}_{n+1/2} \tag{2.6}$$

$$\boldsymbol{p}_{n+1} = \boldsymbol{p}_{n+1/2} + \frac{h}{2m} s(\boldsymbol{p}_{n+1/2}, \boldsymbol{q}_{n+1}) \boldsymbol{f}_{n+1} \tag{2.7}$$

$$t_{n+1} = t_n + h\varrho \tag{2.8}$$

Leimkuhler derived equations (2.5)-(2.7) from the symplectic two-stage order-2 tableau while applying the *sundman* transformations to the PRK formulation [**20**]. The resulting algorithm above introduces coefficients that scale nonlinearly in time depending on the functional form of $s(q(\tau), p(\tau))$. Note that the expressions reduce down to the traditional SV method when the time scaling model is unity, $s(\boldsymbol{p}, \boldsymbol{q}) = 1$, thus confirming that this belongs to the second order Labatto IIIa-b method.

The IAV scheme is made semi-explicit or fully implicit depending on the choice of $s(q, p)$ or $s(q)$. The first choice to depend on q and p renders $p_{n+1/2}$ and q_{n+1} implicit, and consequently the overall IAV scheme becomes more computationally inefficient. Solving for the implicit terms, such as in the case when $p_{n+1/2} = p_n + \frac{h}{2m} s(p_{n+1/2}, q_n) f_n$ can be solved iteratively via the residual difference method below,

$$\frac{\| p_{n+1/2}^{\tilde{n}+1} - p_{n+1/2}^{\tilde{n}} \|}{p_{n+1/2}^{\tilde{n}+1}} < \epsilon \tag{2.9}$$

as done in the Calvo et. al paper [**7**] or with newton-raphson iterations. Here the $\tilde{n}$ term refers to the intermediate solving iterations for $p_{n+1/2}$, while ϵ refers to the acceptable residual threshold. Once the residual is less than ϵ the value of $p_{n+1/2}^{\tilde{n}+1}$ is accepted. The regular iterative approach does not take much time in a single dimension, however the newton-raphson method may prove to be more computationally efficient in higher dimensions but goes untested here.

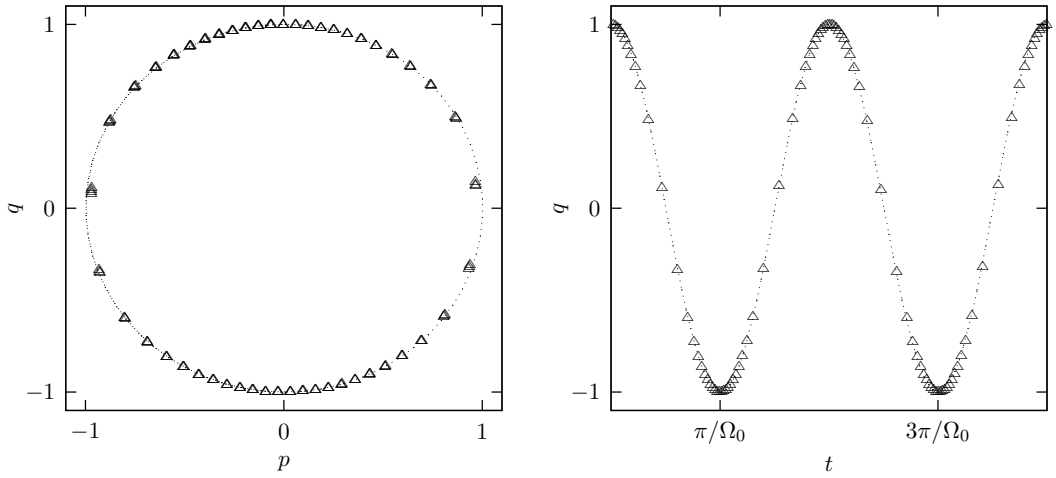

FIGURE 2.1. Represented here in the triangular points is the harmonic IAV trajectory in position q and momentum p, for the exact solution $q(t) = \cos(\Omega_0 t)$ signal. Shown in the left pane is the phase space diagram, and the corresponding position time series is shown in the right panel. The model run was deployed with relatively large parameter settings $h = 10^5$, $h_{\min} = 0.025$ and $h_{\max} = 0.5$. The integrator was configured for bounded time transformation s_ζ with the bounding parameter $\zeta = 0.1$. The exact solution is demonstrated as the dotted line.

Choosing to rely solely on position in $s(q)$ is more computationally efficient and scales as a function of the potential energy surface. In this case the only implicit situation is due to $q_{n+1} = q_n + h\left(\frac{s(p_{n+1/2}, q_n) + s(p_{n+1/2}, q_{n+1})}{2}\right) p_{n+1/2}$, where again we follow the residual difference demonstrated by Calvo et. al.

$$\frac{\|q_{n+1}^{\tilde{n}+1} - q_{n+1}^{\tilde{n}}\|}{\|q_{n+1}^{\tilde{n}+1}\|} < \epsilon \tag{2.10}$$

For the purposes of this study, modeling the harmonic oscillator, we utilize s_ζ as discussed in section 1.3. Note that sampling techniques during the adaptive Verlet procedure are difficult due to unequal spacing in time.

Time averaging with variable timestep techniques may come with an inherit bias. It should be noted that timestep variation means non-equispaced positional points in time and thus leads to biased situations where more samples are taken from moments of fast momenta or high gradient potential curvature. Pooling near low gradients in the harmonic oscillator as shown in Figure 2.1 demonstrates the case of gathering more samples near relaxed force situations. The figure is an example where more simulation iterations are spent near or in lower potential gradient situations.

This may place a large bias on sampling statistics, which may benefit or hinder the average total energy. As mentioned before the accuracy of the position and velocity Verlet depends on the given set of initial conditions [**21**], thus sampling more in regions where accuracy is higher may lead to better results, where the converse of this is also a possibility. In Chapter 3 the average total energy is sampled every iteration and may have some bias, but meets expectations.

2.2. Explicit Adaptive Verlet

After implicit adaptive techniques were introduced in the late 90s, a new explicit method was introduced in the early 2000s [**19**]. Though this method loses generality and symplectic properties, this Explicit Adaptive Verlet (EAV) minimizes the necessity to re-compute the potential multiple times per step.

$$\boldsymbol{p}_{n+1/2} = \boldsymbol{p}_n + \frac{h}{2\rho_n}\boldsymbol{f}_n \tag{2.11}$$

$$\boldsymbol{q}_{n+1/2} = \boldsymbol{q}_n + \frac{h}{2\rho_n}\boldsymbol{p}_{n+1/2} \tag{2.12}$$

$$\rho_{n+1} = 2s(\boldsymbol{p}_{n+1/2}, \boldsymbol{q}_{n+1/2}) - \rho_n \tag{2.13}$$

$$\boldsymbol{q}_{n+1} = \boldsymbol{q}_{n+1/2} + \frac{h}{2\rho_{n+1}}\boldsymbol{p}_{n+1/2} \tag{2.14}$$

$$\boldsymbol{p}_{n+1} = \boldsymbol{p}_{n+1/2} + \frac{h}{2\rho_{n+1}}\boldsymbol{f}_{n+1} \tag{2.15}$$

The equations (2.11)-(2.15) showcase the sequentially ordered set of Verlet procedural steps for advancing position q and momenta p. The first iteration is solved with $\rho_0 = s(q_0)$.

The scheme boils down to a composition method of the symplectic first order method and its adjoint. As described in Leimkuhler's paper this method is symmetric for $s(q,p) = s(q,-p)$ but not symplectic and thus not area preserving. This scheme is not tested here but serves as evidence that there are myriads of additional schemes which are designed to vary the timestep.

2.3. Implementation

In order to computationally deploy the adaptive Verlet scheme in (2.5)-(2.7) a `C++` shared library was created.

The library was created to handle integrators of the Verlet type. In particular the IAV methods (2.5)-(2.7) are computed sequentially but benefit from shared memory operations, such as dot operations. The Basic Linear Algebra Subprograms (BLAS) library was leveraged to help speed up implicit iterations of $\boldsymbol{p}_{n+1/2}$ when norms of the forces are required. The program then performs the secondary step of solving $\boldsymbol{q}_{n+1}$ explicitly by utilizing the result from $\boldsymbol{p}_{n+1/2}$. As mentioned, Calvo et. al. suggests a convenient iterative method for satisfying implicit terms such as $\boldsymbol{p}_{n+1/2}$ and $\boldsymbol{q}_{n+1}$ [**7**]. There are of course more efficient techniques (ie. Bisection or Newton-Raphson methods); however, for comparability with previous studies this article employs the same iterative scheme with residual tolerance of $\varepsilon = 10^{-7}$.

Deploying these algorithms in `C++` were embedded within our own custom framework to offer very fast computational speed, but also to serve as an expandable framework for other integrators in the future. For new developers there are build instructions available on GitHub, where examples are also included. The library is easily built and compiled using the `cmake` utility and is available as an educational open-source integrator repository. As of the time of writing here the IAV, EAV, and SV methods are fully operational.

CHAPTER 3

The Variable Timestep Harmonic Oscillator

Pioneering authors on variable-discrete timestep methods almost always benchmarked their methods on the Kepler problem for orbital mechanics. Determining their discrete integrators efficacy was usually demonstrated using an analysis of the global error [**15**] [**20**] [**7**] [**19**]. Among these tests one of the more interesting focused on the application of the double pendulum and showed variable timesteps had greater stability near cusps and minimized the number of iterations required to simulate pendulum dynamics [**20**]. Notably, the aspect that is not quantified, is the discrete timestep stability range. Rather than bench-marking the IAV method on the traditional Kepler problem, the harmonic oscillator is chosen to represent a linear system. This system is a very well known and is ideal for testing energy stability, as well as characterizing spectra response. A linear stability derivation is presented for the IAV method and compared with findings. Presented here are the considerations that should be carefully examined when using variable timestep methods.

3.1. HMO: IAV Integration

The implicit variable timestep scheme tested here introduces nonlinear s terms that redefine where the underlying method's stability limit lies. It is commonly known where the Størmer-Verlet method's stability limit lies, but due to the influence of s the IAV's stability limit has a different outcome that is not well documented. For the initial conditions $q_0 = 1$ and $p_0 = 0$ we search for the limit of $h_{\max}$ where energy is no longer conservative for the pendulum Hamiltonian shown in (3.1).

$$H(q,p) = \frac{1}{2}p^2/m + \frac{1}{2}kq^2 = \text{const.} \tag{3.1}$$

$$\Omega_0 = \sqrt{k/m}$$

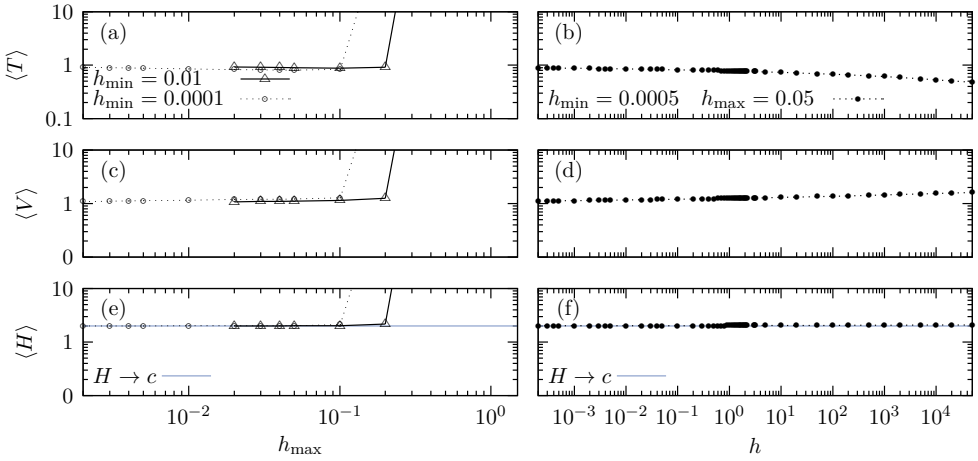

FIGURE 3.1. The left panes (a), (c), and (e) represent the search for the maximum stable timestep h_{hmax} depending on the minimum timestep $h_{\min}$ setting. The triangular marker points correspond with a maximum timestep sweep at a fixed minimum timestep of $h_{\min} = 0.01$, while the circular marker points correspond to runs with a decade smaller scale of $h_{\min} = 0.0001$. The right panels (b), (d), and (f) show extreme values of fictive timestep h for fixed variable timestep range. The averaged total energy aligned with the expected constant energy show in blue and given by equation (3.1). Each simulation in the left panes are given parameters $\Omega_0 = 2$, $h = 1$, and iterates until 10^5 periods are complete.

We tested the stability of the harmonic model with the s_ζ transformation and observe the approximate limit is obeyed as shown in panel (e) of Figure 3.1. The maximum timestep sweeps (a), (c), and (e) show that the approximate upper limit $2/\Omega_0$ is obeyed, although the averaged kinetic and potential energies blow up ten times earlier than predicted. A stable maximum timestep appears to approximately approach $h_{\max} = 0.1$ instead of 1 for the frequency $\Omega_0 = 2$.

Reasoning for the early loss of stability is primarily due to non-linear effects that are not predicted in the linear analysis explained in the next section 3.2. In the future s_ζ can be shaped to fulfill the complex constraint (B.6) given in the appendix using a set of stable trajectories.

Large changes to the fictive timestep h observed in Figure 3.1, panels (b), (d), (f), show disturbances in the kinetic and potential energy portions of the ensemble energy. Increases to h in the functional s_ζ are equivalent to making the ratios W and w large enough to create cusps in the transformation. It seems that despite these cusps the overall performance in the linear model show relatively small but steady time averaged kinetic energy decreases. This could show more prevalent disturbances in non-linear models such as the Lennard Jones. The kinetic energy was

always problematic but becomes worse as h is increased which consequently is one parameter for achieving greater time domain increases. It is important not to fall prey to increasing h too far, in order to achieve speed increases.

3.2. HMO: IAV Linear Stability Criteria

In addition to the brute force stability search, an analytic inequality for the relationship between s and the pendulum's primary frequency Ω_0 is sought in this section. The challenge of finding a limit on $h_{\max}$ must be considered when using time adaptive techniques. Deriving a closed form expression for how large this value can be is critical for yielding the correct energies.

We apply a linear stability approach to finding amplification factor λ which can be applied to non-linear discrete methods [**18**]. Obtaining the amplification factor serves as an estimate indicating unacceptably large errors as a function of the timestep maxima.

$$|\lambda| = \left| \frac{q_{n+1}}{q_n} \right| \leq 1 \tag{3.2}$$

Though in our case we seek to find the error in q and p between timesteps. The time-stepping procedure is stable when the amplitude of λ or complex conjugate is on or within the radius of the unit circle. Additionally, the error of the discrete method must simultaneously be determined for q and p.

$$\lambda = \frac{q_{n+1}}{q_n} \quad \text{and} \quad \lambda = \frac{p_{n+1}}{p_n} \tag{3.3}$$

We satisfy both of this criteria by systematically grouping terms in (2.6) and (2.7). In doing so we obtain a system of equations that can be represented as an Eigenvalue problem. λ Has a corresponding characteristic matrix $\mathcal{V}$ depending on the coefficients in front of q and p found in the integrator itself.

$$\begin{pmatrix} q_{n+1} \\ p_{n+1} \end{pmatrix} = \lambda \begin{pmatrix} q_n \\ p_n \end{pmatrix} \tag{3.4}$$

Solving for λ by diagonalization is typically applied to a linearized system given by the Hookes potential ($f = -\nabla V = -kq$); however, s_ζ or in general $s(q)$ serves as a non-linear functional. Additionally λ does not have a trivially solvable expression due to the implicit terms in the IAV methods. Thus the system is treated linearly by asserting the nonlinear contributions $s(q)$ are constant. Deriving the roots λ and full algebraic steps for the stability criteria can be seen in Appendix A and B. The resulting harmonic stability analysis for the Verlet scheme is of course the inequality below,

$$\Omega_0 h < 2 \tag{3.5}$$

stating that the timestep must be below this non-dimensionalized threshold. When the same method of diagonalization is applied to the IAV method (shown in Appendix B) the resulting Eigenvalues of the IAV scheme indicate a dependence on the scaling function.

$$\Omega_0 h < \frac{2^2}{(s_n + s_{n+1})} \tag{3.6}$$

Obviously reverting back to the SV method by inputting $s = 1$ into (3.6) will reduce the expression to the SV limit.

In order to obtain an approximate limit we make assumptions for s_ζ in an extremely low gradient potential scenario. In this case the scaling function is maximized with $s = 1/m$, and s_n and s_{n+1} are suitably close to each other ($s_n = s_{n+1}$). Utilizing (3.6) and simplifying one step further with our above assumptions lead to the recognizable expression (3.7).

$$2\cancel{s_n}^{1/w}(\Omega_0 h) \leq 2^2 \longrightarrow h_{\max}\Omega_0 \leq 2 \tag{3.7}$$

The limit effectively means the other timestep values below this maximum limit are suitable. In our assumptions made, the alternative situation where s_n and s_{n+1} are not close to each other and $s_n << s_{n+1}$ being true would effectively remove the factor of two in front of $1/w$ and seemingly double the limit on $h_{\max}$. This type of situation is likely due to a sharp decrease in potential and would result in a large position step that could increase the likelihood of particle overlap. The

hopes of avoiding this type of situation are that the particles maintain constant intermolecular contact for smooth time scaling.

3.3. HMO: IAV Spectral Response

Using the same potential energy as section 3.2, we integrate the dynamics of a singular harmonic with the IAV method and have recovered a polychromatic spectra. In testing the frequency response of the IAV, the functional s_ζ is our chosen time-scaler for reasons mentioned in 1.3.

The dynamics are given by the solution

$$q_n = q_0 e^{\pm i\Omega_0 t_n} \tag{3.8}$$

where the natural frequency is defined as $\Omega_0 = \sqrt{k/m}$ for spring coefficient k, mass m, and subscript n denotes the time index.

In this case, a true harmonic integrator should resonate at the singularly given frequency of Ω_0, however the implicit scheme used herein contains other frequencies. We verified the traces of these auxiliary frequencies using three processing methods: a brute force (1) discrete Fourier Transform, (2) the kernel based Non-Uniform Fast Fourier Transform, and (3) the Least Squares method.

The unweighted Fourier Transform $\mathcal{F}$

$$\mathcal{F}\left[q(t)\right] = Q(\omega) = \int_{-\infty}^{\infty} q(t) e^{i\omega t} dt \tag{3.9}$$

must be made discrete and adapted for nonequispaced sampled data [**11**]. Each model run samples N positions and is integrated with a timestep range that satisfies the critical Nyquist sampling frequency ω_c.

$$\omega_c = 2\pi \left(\frac{1}{2|h_{\max}|} \right) \tag{3.10}$$

The critical sampling frequency is conservatively estimated by the largest timestep $h_{\max}$. Thus in our FT spectral scans the set of frequencies span the range (3.11).

$$0 < \omega_m < \omega_c \tag{3.11}$$

We define a linear set of frequencies indexed by integers $m = 1, 2, \ldots, M$ and define a set of unequally spaced timesteps $h_n = t_n - t_{n-1}$ that vary across the time index n.

$$\omega_m = 2\pi \left(\frac{m}{M}\right) \omega_c \tag{3.12}$$

3.3.1. NU-FFT Analysis. The discrete Fourier Transform (3.13) is computationally expensive and requires two loops that carry the numerical complexity of $\mathcal{O}(NM)$.

$$\mathcal{F}_m [q_n] = Q_{m,n} = \frac{1}{N} \sum_{n=0}^{N-1} q_n e^{i\omega_m t_n} \tag{3.13}$$

In order to increase our frequency resolution we compute $N \propto 10^6$ non-uniform points. Using a Non-Uniform Fast Fourier Transform (NU-FFT) based on Dutt and Rokhlin's seminal work relating the complex exponential to a Gaussian interpolator, we reduce the computational cost to $\mathcal{O}(M|\log \varepsilon|^d + NlogN)$. Here ε is the tolerance [**12**]. The modern NU-FFT method used here is based on the exponential of a semicircle kernel optimized for exponential error convergence [**1**]. Essentially the non-equidistant time series treatment between intervals is smoothed by the kernel on a finely defined grid, essentially mapping non-equispaced series onto a regularly spaced interval. This concept has been refined to perform in parallel and with reduced memory thus making the scheme extremely efficient.

In Figure 3.2 we were surprised by a set of additional frequencies that appear to show themselves as integer multiples of the primary frequency Ω_0. Additional spectral peaks were first resolved with the traditional discrete FT method, however we decreased the timestep scales to achieve finer resolution in position. It quickly became apparent that the amount of time to compute $N \times M$ operations for $N \approx \mathcal{O}(10^6)$ was not computable within a reasonable time frame. Thus we rely on NU-FFT for analyzing larger data sets for a set of $M \geq N$ many frequencies.

In our tests we also used the non-uniform time sequence produced by the IAV method and input this into a perfect sinusoidal signal and then performed the dFT and NU-FFT analysis. Again the additional frequency spectra were detected. These anomalous peaks were then verified with Ordinary Least Squares method.

3.3.2. Least Squares Analysis. Demonstrated in this section is an alternative method of determining spectra of the IAV method using Ordinary Least Squares (OLS) to validate the results of the NU-FFT method.

$$\hat{\boldsymbol{\beta}} = \text{argmin}_{\boldsymbol{\beta}} \|(q_i - \tilde{q}_i(\omega_j)\|^2 \tag{3.14}$$

The minimum sum of square differences between set of harmonic trajectories q_i and our best fit trial function $\tilde{q}_i$ will determine amplitude coefficients corresponding to model form(s) that best describe the harmonic data set.

$$\tilde{q}(\omega) = \boldsymbol{X}(\omega)\boldsymbol{\beta} \tag{3.15}$$

The OLS method is related to the Fourier Transform integral by the fact that OLS method sums the distances between trial data q_i and the trial function. For harmonic models that contain solutions at discrete frequency points, this effectively means non-zero terms in the trial function are expected to occur at the harmonic system's natural frequency Ω_0. To find these occurrences the OLS method is performed at incrimental frequencies ω_j, such that Ω_0 is also included.

When the OLS method is applied to integer cycles of harmonic motion, the out of phase trial functions will be flattened to a line in order to minimize the squared sum of the distances. Essentially frequencies that are similar or close to the given cosine distribution q_i will contain non-zero model amplitudes, while out of phase frequencies will be ignored.

$$\boldsymbol{X} = \begin{bmatrix} 1 & \cos(\omega t_0) \\ 1 & \cos(\omega t_1) \\ \vdots & \\ 1 & \cos(\omega t_n) \end{bmatrix} \tag{3.16}$$

To ensure the model matrix contains at-least one solution satisfying IAV harmonics, $\boldsymbol{X}$ is composed of a trial cosine function as shown in equation (3.16). It seemed obvious that a cosine distribution should be included within the model matrix for harmonic motion, since the initial

conditions $q_0 = 1$ and $p_0 = 0$ satisfy the cosine distribution at time $t = 0$. The linear intercept is included as an additional term in the trial model, but β_0 was found to be null in most cases.

Here in this study the least squares formulation (3.14) is performed with Singular Value Decomposition (SVD). By examining the least squares formulation as a linear problem of the form $q_i \approx \boldsymbol{X}\beta$, the unknown feature set of amplitude coefficients $\boldsymbol{\beta}$ can be solved for via the SVD method which avoids round off errors and singularities. Results found for a harmonic set of IAV trajectories show that the amplitudes plotted in Figure 3.2 reveal the same additional spectral peaks predicted by the NU-FFT method.

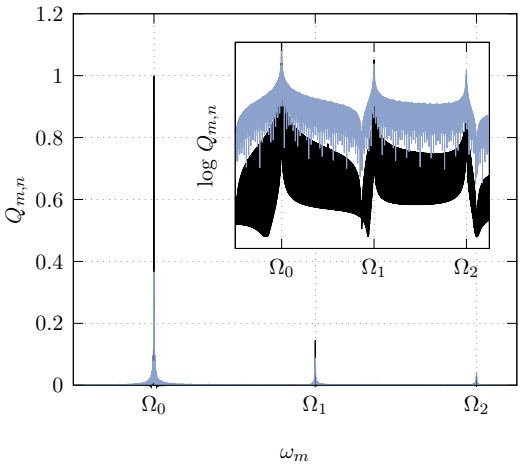

FIGURE 3.2. Shown in black and blue are the IAV spectral results corresponding respectively to least squares and NU-FFT methods. Both spectral techniques show the same anomalous peaks regularly repeating at $\Omega_n = (2n + 1)\Omega_0$. The sample spectra shown here is defined with timestep parameters $h = 1000$, $h_{min} = 0.001$, $h_{\max} = 0.05$ and configured with $s_\zeta = 0.05$ and $\Omega_0 = 1$.

Note that the additional peaks that appear as integer multiples of the natural frequency Ω_0 came as a surprise and hints towards the existence of other solutions contained within the dynamical system introduced by the *sundman* time transformations. Providing the same non-uniform time series to the cosine function still produced the same anomalous peaks and thus deserves further investigation in Chapter 4.

CHAPTER 4

Discussion

Expected frequency behavior for a particle with one degree of freedom demonstrated in Figure 2.1 should yield a singular frequency Ω_0. Contrary to this expectation the time transformative IAV method yields additional spectra as shown in Figure 3.2. It is the purpose of this section to provide the necessary steps required to find a solution for adaptive Verlet motion. Furthermore a loose explanation to the unexpected behavior found in the variable discrete time integration method (IAV) is traced back to the governing differential equation (4.2).

Let us first begin by recalling that the IAV method, (2.5)-(2.7), was designed to satisfy the Hamiltonian constraint which keeps the total system energy constant. The introduction of the time relation $s(q,p)$ modifies the Hamiltonian system to $\tilde{H}$.

$$\tilde{H} = s(q,p)\,(H-\gamma) \quad \text{and} \quad H = 1/2p^T M^{-1} p + V(q). \tag{4.1}$$

The constraint on $s(q,p)$ is that $\tilde{H}$ and H must pass through the same initial solution $\tilde{H}(q_0,p_0) = H(q_0,p_0)$, while γ is some constant. Adjusting to this new Hamiltonian accordingly, the new set of coupled equations for motion is defined in (4.2).

$$\begin{bmatrix} dq/d\tau \\ dp/d\tau \end{bmatrix} = \begin{bmatrix} \nabla_p \tilde{H} \\ -\nabla_q \tilde{H} \end{bmatrix} \tag{4.2}$$

Treating this problem in the same fashion as Leimkuhler [**2**] the formulation of the IAV integrator ignores $\nabla_q s(q,p)$. To clarify, this derivative does not go away since $s(q)$ often depends on position, however we do not adjust the IAV method laid out by Leimkuhler, since we wish to make a direct assessment of the original method.

In order to model harmonic motion the hookes potential is inserted into equation (4.2). In addition the time transformation s must now be chosen to explicitly define the dynamical system.

In most cases the choice of the time transformation $s(q,p) = dt/d\tau$ will define a quasi-linear differential equation [**26**] of the form,

$$\begin{bmatrix} dt/d\tau \\ dq/d\tau \\ dp/d\tau \end{bmatrix} = \mathcal{A} \begin{bmatrix} t \\ q \\ p \end{bmatrix} + \varepsilon g(q, \dot{q}, t) \tag{4.3}$$

where the characteristic matrix $\mathcal{A}$ contains the linear coefficients, and the non-linear terms are premultiplied by a scalar ε (i.e. the discrete timestep h). In our system of equations, the non-linear function g will become apparent after inserting the time relation and expanding the quasi-linear differential equation. Within the scope of this paper we can only determine the linear solution for very selective prescribed conditions.

Let us define a simple form of $s(q)$ and solve for a very confined case where the forces approach zero $\lim_{q\to 0} f(q_n) = 0$. In general this differential equation does not have a trivial solution, especially since the time frames t and τ are mapped non-linearly via position q. Thus this problem becomes very difficult to solve indefinitely without an exact map. In this example we take the time relation to be the arc-length equation (4.4) for the linear system. Where in the limit that position approaches zero the force contributions disappear and thus time variance maps one to one $t \leftrightarrow \tau$.

$$s(q_n) = (1 + \varepsilon \|f_n\|_2) \tag{4.4}$$

It is in this very crude approximation $\lim_{q\to 0} f(q_n) = f_n = 0$ that additional harmonics can be seen. Inserting $s(q_n)$ and expanding our system of equations in terms of position begins to resemble the Van der Pol equation in relation (4.5).

$$\frac{d^2 q}{d\tau^2} + \Omega_0^2 q = \varepsilon g(q, \dot{q}, \varepsilon) \tag{4.5}$$

The non-linear terms in g were found to be the following.

$$g(q, \dot{q}, \tau) = -\Omega_0 \left(2\varepsilon q^2 + \varepsilon^2 k^2 q^3\right) + \varepsilon \left(\frac{k}{1+\varepsilon}\right) \frac{dq}{d\tau} \tag{4.6}$$

Conveniently as the limit defined before is approached, the first few terms in g are reduced and so the only remaining term is the momenta derivative $g \approx dq/d\tau$. Finally a solution to this

non-homogeneous differential equation can be solved for by variation of parameters, which gives the solution as a combination of the unperturbed solution and the particular solution. First the unperturbed solution is found for $g = 0$ which yields the independent solutions $q_1 = c_1 \cos(\Omega_0 \tau)$ and $q_2 = c_2 \sin(\Omega_0 \tau)$. Determining the particular solution is done so via variation of parameters shown below, where the Wronskian term is $W = \Omega_0 c_1 c_2$.

$$q_p(\tau) = -q_1 \int \frac{q_2 g}{W} d\tau + q_2 \int \frac{q_1 g}{W} d\tau \tag{4.7}$$

The integration above is not determinable until realizing one of the solutions is periodic and belongs to the cosine distribution. Thus the sinusoidal momentum term is $dq/d\tau = \sin(\Omega_0 \tau)$. The situation involved begins with the initial conditions $q_0 = 1$, $p_0 = 0$ and for periodic motion this implies one of the solutions is of the cosine distribution. Finally by solving for the particular solutions we arrive at the following expression.

$$q_p = \frac{1}{2\Omega_0} \tau \cos(\Omega_0 \tau) + \frac{\left(2^2 \Omega_0 + 1\right)}{2^3 \Omega_0^2} \cos(\Omega_0 \tau + \pi/2) + \frac{1}{2^3 \Omega_0^2} \cos(3\Omega_0 + \pi/2) \tag{4.8}$$

In the expression above we observe the $3\Omega_0$ term as another mode or frequency that should be present within the spectra. This prediction is confirmed by simulating periodic motion using the IAV method in combination with the time transformation set by equation (4.4). The resulting spectra can be seen in Figure 4.1, and as confirmed by the panel on the right there is resonance at $\Omega_1 = 3\Omega_0$. Finding the solution in the limit as $q \to 0$ demonstrates the potential for other modes, but does not predict all the possible modes. For instance the $5\Omega_0$ peak was not found in this limit.

It should be noted that at the other limit where $dq/d\tau \to 0$ approaches zero, the harmonic system begins to resemble the same form as the modified **Mathieu** problem. This is often equivalent to a frequency modulation problem shown in section 2.3 of [**26**], but the relation to the system in (4.5) is not fully explored yet, since the transformation $dt/d\tau = s(q)$ renders the mapping between $t \leftrightarrow \tau$ indefinable unless the solution is already known. In general, defining $s(q)$ will generate a non-linear, non-homogeneous differential equation without a closed form solution. Offered by the IAV method is a predictable numerical method for solving this non-linear coupled set of position-momenta equations of motion with time reversibility. As we've shown it may introduce additional

harmonics, but it does so in a predictable manner that is consistent with integer multiples of the fundamental frequencies.

It is possible for the IAV method to rid the spectra of additional harmonics using the IAV integrator. This is achieved when $s = 1$, since the IAV method is reverted back into the Størmer-Verlet and thus shouldn't contain non-linear terms. A test of this will confirm that the overall system of equations revert to the ordinary differential equation representing the harmonic oscillator shown in Figure 4.1. The panel on the left of Figure 4.1 demonstrates expected harmonic behavior,

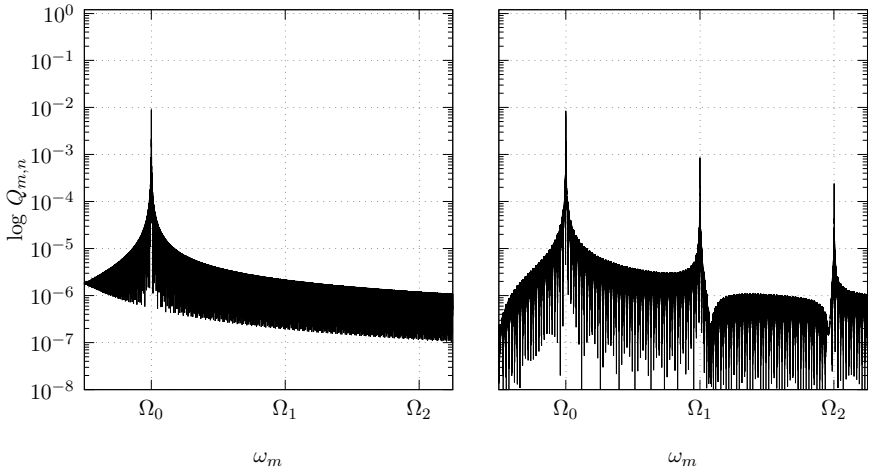

FIGURE 4.1. Shown on the left are spectral modes corresponding $s = 1$ found by the non-uniform FFT technique. Demonstrated on the right panel the spectra produced using $s(q_n) = (1+\varepsilon\|f_n\|_2)$. Both tests were performed with a stable integration step $h = 0.05$ and the frequency $\Omega_0 = 1$.

and that reverting the IAV method back into the form of SV produces a singular harmonic at Ω_0. Introducing the time-scaling factor $s(q)$ has its quirks, however it is a controlled method of scaling the timestep with the added forewarning that non-linearity may affect the spectra. Though when time-scaling is no longer needed, it is always an option to recall the SV method and its symmetric qualities.

CHAPTER 5

Conclusion

In this document programming codes were created to implement variable timestep integrators. The codes march the Implicit Adaptive Verlet integrator forward in time to characterized the energy stability as well as the frequency response for the harmonic system.

Findings in Chapter 3.2 demonstrate that the stability response fell short of the traditional linear stability. The frequency spectra also demonstrated additional harmonics that regularly repeated as integer multiples of the fundamental frequency Ω_0. In Chapter 4 this spectral behavior was been confirmed and analytically derived for the condition that position approaches the origin for the harmonic oscillator.

Overall these differences are due to fundamental differences within the class of differential equations being integrated by the IAV method. Introducing time-transformation functions $s(q)$ into the harmonic system, converts a linear problem into a non-linear differential equation not trivially solved.

Current variable timestep techniques arbitrarily alter the timestep without regard for time-reversibility or symplecticity. By varying the timestep, the Hamiltonian is interchanged in every occurrence [**14**]. The existing time reversible and symplectic adaptive techniques [**15**] [**20**] presented here offer an alternative to brute force timestep varying approaches. They offer a method of controlling the variable timestep while preserving time-reversibility. The forewarning to these methods are that there may be non unique solutions introduced as demonstrated by additional spectral modes. These effects may be mitigated if the fundamental frequency is known, or otherwise $s(q)$ may be set to have no varying timestep effect $s(q) = 1$.

Other areas of careful consideration with the IAV are the choice in s functional. There is room for optimizing the time-transformation functional for greater timestep response depending on potential curvature, but as Chapter 1.3 demonstrates the bounds of the timestep range must be considered.

APPENDIX A

Deriving the Størmer-Verlet λ Factor

Determining the amplification factor λ is used to demonstrate the linear stability. This assessment of the scheme (2.1)-(2.3) requires a linear configuration that the harmonic oscillator provides. The hookes model for linear behavior yields the linear driving force $f_n = -kq_n$ which can be plugged into the integration method.

The system of equations in (3.4) can be solved by finding the Eigenvalues by hand. First we demonstrate this Eigenvalue problem in its characteristic linear system of equations below,

$$\begin{pmatrix} q_{n+1} \\ p_{n+1} \end{pmatrix} = \mathcal{V} \begin{pmatrix} q_n \\ p_n \end{pmatrix} \tag{A.1}$$

where the coefficients in $\mathcal{V}$ represent the terms found in the coupled linear system.

$$\mathcal{V} = \begin{pmatrix} a & b \\ c & d \end{pmatrix} \tag{A.2}$$

For completeness we list the terms of the SV method below.

$$a = \left(1 - \frac{(\Omega_0 h)^2}{2}\right) \tag{A.3}$$

$$b = h \tag{A.4}$$

$$c = h\Omega_0^2 \left(\frac{(\Omega_0 h)^2}{2} - 1\right) \tag{A.5}$$

$$d = \left(1 - \frac{(\Omega_0 h)^2}{2}\right) \tag{A.6}$$

Going through some algebra for the 2×2 Eigenvalue problem yields the following solution.

$$\lambda_{\pm} = \frac{(d+a) \pm \sqrt{(d+a)^2 - 4(ad-cb)}}{2} \tag{A.7}$$

With a little algebra we arrive at an expression for the roots .

$$\lambda_{\pm} = \left(1 - \frac{(\Omega_0 h)^2}{2}\right) \pm i \left(1 - \frac{(\Omega_0 h)^2}{2^2}\right)^{1/2} \Omega_0 h \tag{A.8}$$

The following steps used herin this section are then used in the IAV's stability assessment.

APPENDIX B

Deriving the IAV Scheme's λ Factor

After some rearrangement in equations (2.6) and (2.7) a systematic representation of variable step equations can be derived. For short hand notation the scaling functions $s(p_{n+1/2}, q_n)$ are abridged as s_n and $s(p_{n+1/2}, q_{n+1})$ as s_{n+1}. Thus the same method shown in Appendix A is used to determine the amplification factor. Begin with the matrix coefficients:

$$a = \left(1 - \frac{(\Omega_0 h)^2}{2}\left(\frac{s_n^2 + s_{n+1}s_n}{2}\right)\right) \tag{B.1}$$

$$b = h\left(\frac{s_n + s_{n+1}}{2}\right) \tag{B.2}$$

$$c = h\Omega_0^2\left(\frac{(\Omega_0 h)^2}{2}\left(\frac{s_n s_{n+1}}{2}\right) - 1\right)\left(\frac{s_{n+1} + s_n}{2}\right) \tag{B.3}$$

$$d = \left(1 - \frac{(\Omega_0 h)^2}{2}\left(\frac{s_n s_{n+1} + s_{n+1}^2}{2}\right)\right) \tag{B.4}$$

Plugging these coefficients into equation (A.7) we arrive at the result below.

$$\lambda_\pm = \left(1 - \frac{(\Omega_0 h)^2}{2}\left(\frac{s_n + s_{n+1}}{2}\right)^2\right) \pm i\left(1 - \frac{(\Omega_0 h)^2}{2^2}\left(\frac{s_n + s_{n+1}}{2}\right)^2\right)^{1/2} \Omega_0 h\left(\frac{s_n + s_{n+1}}{2}\right) \tag{B.5}$$

We know that these roots are being derived for periodic motion, and thus it's solution or the complex conjugate of the roots λ must lie exactly on the unit circle for all time. However to traverse the unit circle, the complex component must be preserved. Thus the inequality,

$$\left(1 - \left(\frac{\Omega_0 h}{2}\right)^2\left(\frac{s_n + s_{n+1}}{2}\right)^2\right)^{1/2} > 0 \tag{B.6}$$

preserves the complex component necessary for stability as time is evolved. Using the inequality an overall stability limit can be derived for h. By holding the non-linear coefficients constant we arrives at the expression (B.7). This serves as a conservative estimate for choosing h within the limits determined by $|s_n| \approx |s_{n+1}| = h/h_{max}$.

$$h \leq \frac{2^2}{\Omega_0 \left(s_n + s_{n+1}\right)} \tag{B.7}$$

Treating the amplification factor as linear by holding the non-linear coefficients s constant is a rudimentary yet necessary step in assessing the overall viability of the method's stability. If the method does not pass the rudimentary test, it does not have much hope of passing a more detailed assessment over all the states q_n.

Bibliography

[1] A. H. Barnett, J. Magland, and L. af Klinteberg, *A parallel nonuniform fast fourier transform library based on an "exponential of semicircle" kernel*, SIAM Journal on Scientific Computing, 41 (2019), pp. C479–C504.

[2] E. Barth, B. Leimkuhler, and S. Reich, *A time-reversible variable-stepsize integrator for constrained dynamics*, SIAM journal on scientific computing, 21 (1999), pp. 1027–1044.

[3] A. P. Bartók, M. C. Payne, R. Kondor, and G. Csányi, *Gaussian approximation potentials: the accuracy of quantum mechanics, without the electrons*, Physical review letters, 104 (2010), pp. 136403–136403.

[4] K. M. Beardmore and N. Grønbech-Jensen, *An efficient molecular dynamics scheme for predicting dopant implant profiles in semiconductors*, Nuclear Instruments and Methods in Physics Research Section B: Beam Interactions with Materials and Atoms, 153 (1999), pp. 391–397.

[5] J. Behler and M. Parrinello, *Generalized neural-network representation of high-dimensional potential-energy surfaces*, Phys. Rev. Lett., 98 (2007), p. 146401.

[6] J. C. Butcher, *Numerical Methods for Ordinary Differential Equations*, John Wiley Sons, Ltd, Chichester, UK, 2008.

[7] M. Calvo, M. López-Marcos, and J. Sanz-Serna, *Variable step implementation of geometric integrators*, Applied numerical mathematics, 28 (1998), pp. 1–16.

[8] M. P. CALVO and J. M. SANZ-SERNA, *The development of variable-step symplectic integrators, with application to the two-body problem*, SIAM journal on scientific computing, 14 (1993), pp. 936–952.

[9] N. C. Cole-Filipiak, R. Knepper, M. Wood, and K. Ramasesha, *Mode-selective vibrational energy transfer dynamics in 1, 3, 5-trinitroperhydro-1, 3, 5-triazine (rdx) thin films*, The Journal of Physical Chemistry A, 125 (2021), pp. 7788–7802.

[10] M. Cusentino, M. Wood, and A. Thompson, *Beryllium-driven structural evolution at the divertor surface*, Nuclear fusion, 61 (2021), pp. 46049–.

[11] T. J. Deeming, *Fourier analysis with unequally-spaced data*, Astrophysics and Space Science, 36 (1975), pp. 137–158.

[12] A. Dutt and V. Rokhlin, *Fast fourier transforms for nonequispaced data*, SIAM Journal on Scientific computing, 14 (1993), pp. 1368–1393.

[13] S. Geng, *Symplectic partitioned runge-kutta methods*, Journal of Computational Mathematics, (1993), pp. 365–372.

[14] B. Gladman, M. Duncan, and J. Candy, *Symplectic integrators for long-term integrations in celestial mechanics*, Celestial Mechanics and Dynamical Astronomy, 52 (1991), pp. 221–240.

[15] E. Hairer, *Variable time step integration with symplectic methods*, Applied Numerical Mathematics, 25 (1997), pp. 219–227. Special Issue on Time Integration.

[16] E. E. Hairer, *Geometric numerical integration : structure-preserving algorithms for ordinary differential equations*, Springer series in computational mathematics, 31, Springer, Berlin ;, 2nd ed ed., 2006.

[17] K. D. Hammond and B. D. Wirth, *Erratum: "crystal orientation effects on helium ion depth distributions and adatom formation processes in plasma-facing tungsten" [j. appl. phys. 116, 143301 (2014)]*, Journal of Applied Physics, 118 (2015), p. 229901.

[18] C. Hirsch, *Numerical computation of internal and external flows*, Computational methods for inviscid and viscous flows, 2 (1990).

[19] T. Holder, B. Leimkuhler, and S. Reich, *Explicit variable step-size and time-reversible integration*, Applied Numerical Mathematics, 39 (2001), pp. 367–377. Themes in Geometric Integration.

[20] W. Huang and B. Leimkuhler, *The adaptive verlet method*, SIAM Journal on Scientific Computing, 18 (1997), pp. 239–256.

[21] L. F. G. Jensen and N. Grønbech-Jensen, *Accurate configurational and kinetic statistics in discrete-time langevin systems*, Molecular Physics, 117 (2019), pp. 2511–2526.

[22] B. Leimkuhler, *Reversible adaptive regularization: Perturbed kepler motion and classical atomic trajectories*, Philosophical Transactions: Mathematical, Physical and Engineering Sciences, 357 (1999), pp. 1101–1133.

[23] T. Levi-Civita, *Sur la résolution qualitative du problème restreint*, Acta Mathematica, 30 (1906), p. 305.

[24] D. A. D. A. McQuarrie, *Statistical mechanics*, University Science Books, Sausalito, Calif, 2000.

[25] S. J. Plimpton and A. P. Thompson, *Computational aspects of many-body potentials*, MRS bulletin, 37 (2012), pp. 513–521.

[26] J. A. J. A. Sanders, *Averaging methods in nonlinear dynamical systems*, Applied mathematical sciences ; v. 59, Springer, New York, 2nd ed. ed., 2007.

[27] J. Sanz-Serna, *Symplectic runge-kutta and related methods: recent results*, Physica D: Nonlinear Phenomena, 60 (1992), pp. 293–302.

[28] D. Stoffer and K. Nipp, *Invariant curves for variable step size integrators*, BIT, 31 (1991), pp. 169–180.

[29] K. F. Sundman, *Mémoire sur le problème des trois corps*, Acta mathematica, 36 (1913), pp. 105–179.

[30] A. Thompson, L. Swiler, C. Trott, S. Foiles, and G. Tucker, *Spectral neighbor analysis method for automated generation of quantum-accurate interatomic potentials*, Journal of Computational Physics, 285 (2015), pp. 316–330.

[31] L. Verlet, *Computer "experiments" on classical fluids. i. thermodynamical properties of lennard-jones molecules*, Phys. Rev., 159 (1967), pp. 98–103.

[32] M. A. Wood, M. A. Cusentino, B. D. Wirth, and A. P. Thompson, *Data-driven material models for atomistic simulation*, Phys. Rev. B, 99 (2019), p. 184305.

[33] J. F. J. F. Ziegler, *SRIM, the stopping and range of ions in matter*, SRIM Co., Chester, Maryland, 2008.

[34] Y. Zuo, C. Chen, X. Li, Z. Deng, Y. Chen, J. Behler, G. Csányi, A. V. Shapeev, A. P. Thompson, M. A. Wood, and S. P. Ong, *A performance and cost assessment of machine learning interatomic potentials*, (2019).